

BABAR-CONF-00/13
SLAC-PUB-8535

Study of inclusive $D_s^{(*)\pm}$ production in B decays and measurement of $B^0 \rightarrow D^{*-}D_s^{(*)+}$ decays using a partial reconstruction technique

The *BABAR* Collaboration

July 25, 2000

Abstract

Electron-positron annihilation data collected by the *BABAR* detector near the $\Upsilon(4S)$ resonance are used to study the inclusive decay of B mesons to D_s^\pm and $D_s^{*\pm}$ mesons, where the D_s^\pm is reconstructed using the decay $D_s^\pm \rightarrow \phi\pi^\pm$. The production fraction of inclusive $D_s^{(*)\pm}$ and the corresponding momentum spectra have been determined. The exclusive decays $B^0 \rightarrow D^{*-}D_s^{(*)+}$ are observed with a partial reconstruction technique which uses the soft pion from the $D^{*\pm}$ decay in association with the reconstructed $D_s^{(*)\pm}$. The beam energy constraint is used to determine the missing mass recoiling against the D_s^\pm system, showing a clear signal for this process. From the observed rates, preliminary results for the corresponding branching fractions have been obtained.

Submitted to the XXXth International Conference on High Energy Physics, Osaka, Japan.

The *BABAR* Collaboration

B. Aubert, A. Boucham, D. Boutigny, I. De Bonis, J. Favier, J.-M. Gaillard, F. Galeazzi, A. Jeremie,
Y. Karyotakis, J. P. Lees, P. Robbe, V. Tisserand, K. Zachariadou

Lab de Phys. des Particules, F-74941 Annecy-le-Vieux, CEDEX, France

A. Palano

Università di Bari, Dipartimento di Fisica and INFN, I-70126 Bari, Italy

G. P. Chen, J. C. Chen, N. D. Qi, G. Rong, P. Wang, Y. S. Zhu

Institute of High Energy Physics, Beijing 100039, China

G. Eigen, P. L. Reinertsen, B. Stugu

University of Bergen, Inst. of Physics, N-5007 Bergen, Norway

B. Abbott, G. S. Abrams, A. W. Borgland, A. B. Breon, D. N. Brown, J. Button-Shafer, R. N. Cahn,
A. R. Clark, Q. Fan, M. S. Gill, S. J. Gowdy, Y. Groysman, R. G. Jacobsen, R. W. Kadel, J. Kadyk,
L. T. Kerth, S. Kluth, J. F. Kral, C. Leclerc, M. E. Levi, T. Liu, G. Lynch, A. B. Meyer, M. Momayezi,
P. J. Oddone, A. Perazzo, M. Pripstein, N. A. Roe, A. Romosan, M. T. Ronan, V. G. Shelkov, P. Strother,
A. V. Telnov, W. A. Wenzel

Lawrence Berkeley National Lab, Berkeley, CA 94720, USA

P. G. Bright-Thomas, T. J. Champion, C. M. Hawkes, A. Kirk, S. W. O'Neale, A. T. Watson, N. K. Watson
University of Birmingham, Birmingham, B15 2TT, UK

T. Deppermann, H. Koch, J. Krug, M. Kunze, B. Lewandowski, K. Peters, H. Schmuecker, M. Steinke
Ruhr Universität Bochum, Inst. f. Experimentalphysik 1, D-44780 Bochum, Germany

J. C. Andress, N. Chevalier, P. J. Clark, N. Cottingham, N. De Groot, N. Dyce, B. Foster, A. Mass,
J. D. McFall, D. Wallom, F. F. Wilson
University of Bristol, Bristol BS8 1TL, UK

K. Abe, C. Hearty, T. S. Mattison, J. A. McKenna, D. Thiessen
University of British Columbia, Vancouver, BC, Canada V6T 1Z1

B. Camanzi, A. K. McKemey, J. Tinslay
Brunel University, Uxbridge, Middlesex UB8 3PH, UK

V. E. Blinov, A. D. Bukin, D. A. Bukin, A. R. Buzykaev, M. S. Dubrovin, V. B. Golubev,
V. N. Ivanchenko, A. A. Korol, E. A. Kravchenko, A. P. Onuchin, A. A. Salnikov, S. I. Serednyakov,
Yu. I. Skoppen, A. N. Yushkov

*Budker Institute of Nuclear Physics, Siberian Branch of Russian Academy of Science, Novosibirsk 630090,
Russia*

A. J. Lankford, M. Mandelkern, D. P. Stoker
University of California at Irvine, Irvine, CA 92697, USA

A. Ahsan, K. Arisaka, C. Buchanan, S. Chun
University of California at Los Angeles, Los Angeles, CA 90024, USA

J. G. Branson, R. Faccini,* D. B. MacFarlane, Sh. Rahatlou, G. Raven, V. Sharma
University of California at San Diego, La Jolla, CA 92093, USA

C. Campagnari, B. Dahmes, P. A. Hart, N. Kuznetsova, S. L. Levy, O. Long, A. Lu, J. D. Richman,
W. Verkerke, M. Witherell, S. Yellin
University of California at Santa Barbara, Santa Barbara, CA 93106, USA

J. Beringer, D. E. Dorfan, A. Eisner, A. Frey, A. A. Grillo, M. Grothe, C. A. Heusch, R. P. Johnson,
W. Kroeger, W. S. Lockman, T. Pulliam, H. Sadrozinski, T. Schalk, R. E. Schmitz, B. A. Schumm,
A. Seiden, M. Turri, D. C. Williams

University of California at Santa Cruz, Institute for Particle Physics, Santa Cruz, CA 95064, USA

E. Chen, G. P. Dubois-Felsmann, A. Dvoretskii, D. G. Hitlin, Yu. G. Kolomensky, S. Metzler, J. Oyang,
F. C. Porter, A. Ryd, A. Samuel, M. Weaver, S. Yang, R. Y. Zhu
California Institute of Technology, Pasadena, CA 91125, USA

R. Aleksan, G. De Domenico, A. de Lesquen, S. Emery, A. Gaidot, S. F. Ganzhur, G. Hamel de
Monchenault, W. Kozanecki, M. Langer, G. W. London, B. Mayer, B. Serfass, G. Vasseur, C. Yeche,
M. Zito

Centre d'Etudes Nucléaires, Saclay, F-91191 Gif-sur-Yvette, France

S. Devmal, T. L. Geld, S. Jayatilleke, S. M. Jayatilleke, G. Mancinelli, B. T. Meadows, M. D. Sokoloff
University of Cincinnati, Cincinnati, OH 45221, USA

J. Blouw, J. L. Harton, M. Krishnamurthy, A. Soffer, W. H. Toki, R. J. Wilson, J. Zhang
Colorado State University, Fort Collins, CO 80523, USA

S. Fahey, W. T. Ford, F. Gaede, D. R. Johnson, A. K. Michael, U. Nauenberg, A. Olivas, H. Park,
P. Rankin, J. Roy, S. Sen, J. G. Smith, D. L. Wagner
University of Colorado, Boulder, CO 80309, USA

T. Brandt, J. Brose, G. Dahlinger, M. Dickopp, R. S. Dubitzky, M. L. Kocian, R. Müller-Pfefferkorn,
K. R. Schubert, R. Schwierz, B. Spaan, L. Wilden
Technische Universität Dresden, Inst. f. Kern- u. Teilchenphysik, D-01062 Dresden, Germany

L. Behr, D. Bernard, G. R. Bonneau, F. Brochard, J. Cohen-Tanugi, S. Ferrag, E. Roussot, C. Thiebaux,
G. Vasileiadis, M. Verderi
Ecole Polytechnique, Lab de Physique Nucléaire H. E., F-91128 Palaiseau, France

A. Anjomshoaa, R. Bernet, F. Di Lodovico, F. Muheim, S. Player, J. E. Swain
University of Edinburgh, Edinburgh EH9 3JZ, UK

C. Bozzi, S. Dittongo, M. Folegani, L. Piemontese
Università di Ferrara, Dipartimento di Fisica and INFN, I-44100 Ferrara, Italy

E. Treadwell
Florida A&M University, Tallahassee, FL 32307, USA

* Jointly appointed with Università di Roma La Sapienza, Dipartimento di Fisica and INFN, I-00185 Roma, Italy

R. Baldini-Ferroli, A. Calcaterra, R. de Sangro, D. Falciai, G. Finocchiaro, P. Patteri, I. M. Peruzzi,[†]
M. Piccolo, A. Zallo

Laboratori Nazionali di Frascati dell'INFN, I-00044 Frascati, Italy

S. Bagnasco, A. Buzzo, R. Contri, G. Crosetti, P. Fabbricatore, S. Farinon, M. Lo Vetere, M. Macri,
M. R. Monge, R. Musenich, R. Parodi, S. Passaggio, F. C. Pastore, C. Patrignani, M. G. Pia, C. Priano,
E. Robutti, A. Santroni

Università di Genova, Dipartimento di Fisica and INFN, I-16146 Genova, Italy

J. Cochran, H. B. Crawley, P.-A. Fischer, J. Lamsa, W. T. Meyer, E. I. Rosenberg
Iowa State University, Ames, IA 50011-3160, USA

R. Bartoldus, T. Dignan, R. Hamilton, U. Mallik
University of Iowa, Iowa City, IA 52242, USA

C. Angelini, G. Batignani, S. Bettarini, M. Bondioli, M. Carpinelli, F. Forti, M. A. Giorgi, A. Lusiani,
M. Morganti, E. Paoloni, M. Rama, G. Rizzo, F. Sandrelli, G. Simi, G. Triggiani

Università di Pisa, Scuola Normale Superiore, and INFN, I-56100 Pisa, Italy

M. Benkebil, G. Grosdidier, C. Hast, A. Hoecker, V. LePeltier, A. M. Lutz, S. Plaszczynski, M. H. Schune,
S. Trincaz-Duvoud, A. Valassi, G. Wormser
LAL, F-91898 ORSAY Cedex, France

R. M. Bionta, V. Brigljević, O. Fackler, D. Fujino, D. J. Lange, M. Mugge, X. Shi, T. J. Wenaus,
D. M. Wright, C. R. Wuest

Lawrence Livermore National Laboratory, Livermore, CA 94550, USA

M. Carroll, J. R. Fry, E. Gabathuler, R. Gamet, M. George, M. Kay, S. McMahon, T. R. McMahon,
D. J. Payne, C. Touramanis
University of Liverpool, Liverpool L69 3BX, UK

M. L. Aspinwall, P. D. Dauncey, I. Eschrich, N. J. W. Gunawardane, R. Martin, J. A. Nash, P. Sanders,
D. Smith

University of London, Imperial College, London, SW7 2BW, UK

D. E. Azzopardi, J. J. Back, P. Dixon, P. F. Harrison, P. B. Vidal, M. I. Williams
University of London, Queen Mary and Westfield College, London, E1 4NS, UK

G. Cowan, M. G. Green, A. Kurup, P. McGrath, I. Scott

University of London, Royal Holloway and Bedford New College, Egham, Surrey TW20 0EX, UK

D. Brown, C. L. Davis, Y. Li, J. Pavlovich, A. Trunov
University of Louisville, Louisville, KY 40292, USA

J. Allison, R. J. Barlow, J. T. Boyd, J. Fullwood, A. Khan, G. D. Lafferty, N. Savvas, E. T. Simopoulos,
R. J. Thompson, J. H. Weatherall

University of Manchester, Manchester M13 9PL, UK

[†] Jointly appointed with Univ. di Perugia, I-06100 Perugia, Italy

C. Dallapiccola, A. Farbin, A. Jawahery, V. Lillard, J. Olsen, D. A. Roberts

University of Maryland, College Park, MD 20742, USA

B. Brau, R. Cowan, F. Taylor, R. K. Yamamoto

Massachusetts Institute of Technology, Lab for Nuclear Science, Cambridge, MA 02139, USA

G. Blaylock, K. T. Flood, S. S. Hertzbach, R. Kofler, C. S. Lin, S. Willocq, J. Wittlin

University of Massachusetts, Amherst, MA 01003, USA

P. Bloom, D. I. Britton, M. Milek, P. M. Patel, J. Trischuk

McGill University, Montreal, PQ, Canada H3A 2T8

F. Lanni, F. Palombo

Università di Milano, Dipartimento di Fisica and INFN, I-20133 Milano, Italy

J. M. Bauer, M. Booke, L. Cremaldi, R. Kroeger, J. Reidy, D. Sanders, D. J. Summers

University of Mississippi, University, MS 38677, USA

J. F. Arguin, J. P. Martin, J. Y. Nief, R. Seitz, P. Taras, A. Woch, V. Zacek

Université de Montréal, Lab. René J. A. Levesque, Montréal, QC, Canada, H3C 3J7

H. Nicholson, C. S. Sutton

Mount Holyoke College, South Hadley, MA 01075, USA

N. Cavallo, G. De Nardo, F. Fabozzi, C. Gatto, L. Lista, D. Piccolo, C. Sciacca

Università di Napoli Federico II, Dipartimento di Scienze Fisiche and INFN, I-80126 Napoli, Italy

M. Falbo

Northern Kentucky University, Highland Heights, KY 41076, USA

J. M. LoSecco

University of Notre Dame, Notre Dame, IN 46556, USA

J. R. G. Alsmiller, T. A. Gabriel, T. Handler

Oak Ridge National Laboratory, Oak Ridge, TN 37831, USA

F. Colecchia, F. Dal Corso, G. Michelon, M. Morandin, M. Posocco, R. Stroili, E. Torassa, C. Voci

Università di Padova, Dipartimento di Fisica and INFN, I-35131 Padova, Italy

M. Benayoun, H. Briand, J. Chauveau, P. David, C. De la Vaissière, L. Del Buono, O. Hamon, F. Le Diberder, Ph. Leruste, J. Lory, F. Martinez-Vidal, L. Roos, J. Stark, S. Versillé

Universités Paris VI et VII, Lab de Physique Nucléaire H. E., F-75252 Paris, Cedex 05, France

P. F. Manfredi, V. Re, V. Speziali

Università di Pavia, Dipartimento di Elettronica and INFN, I-27100 Pavia, Italy

E. D. Frank, L. Gladney, Q. H. Guo, J. H. Panetta

University of Pennsylvania, Philadelphia, PA 19104, USA

M. Haire, D. Judd, K. Paick, L. Turnbull, D. E. Wagoner

Prairie View A&M University, Prairie View, TX 77446, USA

J. Albert, C. Bula, M. H. Kelsey, C. Lu, K. T. McDonald, V. Miftakov, S. F. Schaffner, A. J. S. Smith,
A. Tumanov, E. W. Varnes

Princeton University, Princeton, NJ 08544, USA

G. Cavoto, F. Ferrarotto, F. Ferroni, K. Fratini, E. Lamanna, E. Leonardi, M. A. Mazzoni, S. Morganti,
G. Piredda, F. Safai Tehrani, M. Serra

Università di Roma La Sapienza, Dipartimento di Fisica and INFN, I-00185 Roma, Italy

R. Waldi

Universität Rostock, D-18051 Rostock, Germany

P. F. Jacques, M. Kalelkar, R. J. Plano

Rutgers University, New Brunswick, NJ 08903, USA

T. Adye, U. Egede, B. Franek, N. I. Geddes, G. P. Gopal

Rutherford Appleton Laboratory, Chilton, Didcot, Oxon., OX11 0QX, UK

N. Copty, M. V. Purohit, F. X. Yumiceva

University of South Carolina, Columbia, SC 29208, USA

I. Adam, P. L. Anthony, F. Anulli, D. Aston, K. Baird, E. Bloom, A. M. Boyarski, F. Bulos, G. Calderini,
M. R. Convery, D. P. Coupal, D. H. Coward, J. Dorfan, M. Doser, W. Dunwoodie, T. Glanzman,
G. L. Godfrey, P. Grossi, J. L. Hewett, T. Himel, M. E. Huffer, W. R. Innes, C. P. Jessop, P. Kim,
U. Langenegger, D. W. G. S. Leith, S. Luitz, V. Luth, H. L. Lynch, G. Manzin, H. Marsiske, S. Menke,
R. Messner, K. C. Moffeit, M. Morii, R. Mount, D. R. Muller, C. P. O'Grady, P. Paolucci, S. Petrak,
H. Quinn, B. N. Ratcliff, S. H. Robertson, L. S. Rochester, A. Roodman, T. Schietinger, R. H. Schindler,
J. Schwiening, G. Sciolla, V. V. Serbo, A. Snyder, A. Soha, S. M. Spanier, A. Stahl, D. Su, M. K. Sullivan,
M. Talby, H. A. Tanaka, J. Va'vra, S. R. Wagner, A. J. R. Weinstein, W. J. Wisniewski, C. C. Young

Stanford Linear Accelerator Center, Stanford, CA 94309, USA

P. R. Burchat, C. H. Cheng, D. Kirkby, T. I. Meyer, C. Roat

Stanford University, Stanford, CA 94305-4060, USA

A. De Silva, R. Henderson

TRIUMF, Vancouver, BC, Canada V6T 2A3

W. Bugg, H. Cohn, E. Hart, A. W. Weidemann

University of Tennessee, Knoxville, TN 37996, USA

T. Benninger, J. M. Izen, I. Kitayama, X. C. Lou, M. Turcotte

University of Texas at Dallas, Richardson, TX 75083, USA

F. Bianchi, M. Bona, B. Di Girolamo, D. Gamba, A. Smol, D. Zanin

Università di Torino, Dipartimento di Fisica Sperimentale and INFN, I-10125 Torino, Italy

L. Bosisio, G. Della Ricca, L. Lanceri, A. Pompli, P. Poropat, M. Prest, E. Vallazza, G. Vuagnin

Università di Trieste, Dipartimento di Fisica and INFN, I-34127 Trieste, Italy

R. S. Panvini

Vanderbilt University, Nashville, TN 37235, USA

C. M. Brown, P. D. Jackson, R. Kowalewski, J. M. Roney
University of Victoria, Victoria, BC, Canada V8W 3P6

H. R. Band, E. Charles, S. Dasu, P. Elmer, J. R. Johnson, J. Nielsen, W. Orejudos, Y. Pan, R. Prepost,
I. J. Scott, J. Walsh, S. L. Wu, Z. Yu, H. Zobernig
University of Wisconsin, Madison, WI 53706, USA

1 Introduction

The production of the $D_s^{(*)\pm}$ meson in B decays allows one to study the mechanisms leading to the creation of a $c\bar{s}$ quark pair. The main diagram contributing to this decay is shown in Fig. 1. Other B decay diagrams also contribute, although at a lower level, but no attempt is made to quantify their rate in this paper. As has been pointed out in Ref. [1], the $b \rightarrow c\bar{s}s$ decay rate may be large and could help to explain the theoretical difficulties [2] in accounting simultaneously for the total inclusive B decay rate and the semileptonic branching fraction of the B meson. As a longer term goal, the measurement of the rate and momentum spectrum of D_s^\pm meson produced in B decays beyond the kinematic limit for the process $B \rightarrow D_s^{*+} X_c$ could be used to study $b \rightarrow u$ transitions. Despite the fact that purely hadronic final states are more difficult to understand theoretically, one may use the particular decay described in this paper to extract V_{ub}/V_{cb} [3]. This document reports measurements made with the *BABAR* detector of both the inclusive $D_s^{(*)\pm}$ production rates and momentum spectra in B decays and the branching fractions of two specific two-body B decay modes involving a $D_s^{(*)\pm}$ meson. The latter measurements are made using a partial reconstruction technique.

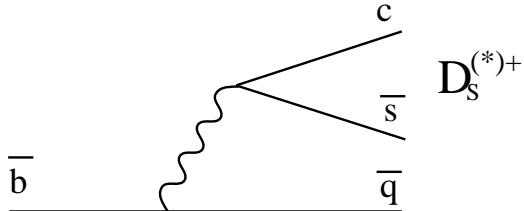


Figure 1: The main spectator diagram leading to the production of $D_s^{(*)\pm}$ mesons in B decays.

2 The detector and the data sample

A description of the *BABAR* detector and the definition of many general analysis procedures can be found in an accompanying paper [4]. Here only the components of the detector most crucial to this analysis are briefly summarized.

Charged particles are detected and their momenta measured by a combination of a central drift chamber (DCH) with a helium-based gas and a five-layer (double-sided) silicon vertex tracker (SVT), embedded in a 1.5 T solenoidal field produced by a superconducting magnet. The charged particle momentum resolution is approximately $(\delta p_T/p_T)^2 = (0.0015 p_T)^2 + (0.005)^2$, where p_T is in GeV/c . The SVT, with typically $10\ \mu\text{m}$ single-hit resolution, provides vertex information in both the transverse plane and in z .

Particles are identified using a combination of measurements from all the *BABAR* components. Charged particle identification exploits ionization energy loss measured in the DCH and SVT as well as Cherenkov radiation measured in a ring imaging detector (DIRC). Electrons and photons are identified by the CsI electromagnetic calorimeter.

Multihadronic events produced in e^+e^- annihilation at the PEP-II collider (SLAC) and collected with the *BABAR* detector have been used in this analysis. These data were taken at the $\Upsilon(4S)$ resonance center of mass energy and at an energy about 40 MeV below the $B\bar{B}$ threshold. The integrated luminosity for on resonance data is $7.73\ \text{fb}^{-1}$ and $1.17\ \text{fb}^{-1}$ for off resonance.

3 Inclusive D_s^\pm production

3.1 D_s^\pm reconstruction

The D_s^\pm mesons are reconstructed using the mode $D_s^\pm \rightarrow \phi\pi^\pm$ with $\phi \rightarrow K^+K^-$. In order to obtain a sufficiently clean sample, particle identification is necessary. To this end, both energy loss (dE/dx) information from the Drift Chamber and the Vertex Detector and the DIRC (a Cherenkov imaging detector) are used to identify the kaons produced in the ϕ decay.

The selection is based on the likelihoods given by each detector and uses, for each track, the ratio of likelihoods for the pion and the kaon mass hypotheses L_π/L_K . If this ratio is less than unity for at least one of the considered subsystems, the particle is selected as a kaon. The DIRC is used both in the positive identification mode and the veto mode. A tighter level of identification is also available using a total likelihood defined as the product of the likelihoods of each subsystem. In this case the track is tagged as a kaon if the ratio of the total likelihoods for the pion and kaon mass hypotheses is less than unity.

Three charged tracks coming from a common vertex are then combined to form a D_s^\pm candidate. Two oppositely-charged tracks have to be identified as kaons, one of these using the basic criteria and the second one using the tighter selection. The K^+K^- invariant mass must be within $8 \text{ MeV}/c^2$ of the nominal ϕ mass (see Fig. 2). In this particular decay, the ϕ meson is polarized longitudinally and therefore the angular distribution of the kaons has a $\cos^2 \theta_H$ dependence, where the θ_H is the angle between the K^+ in the ϕ rest frame and the ϕ direction in the D_s^\pm rest frame. We require $|\cos \theta_H| > 0.3$, thereby keeping 97.5% of the signal while rejecting about 30% of the background.

Using the selection criteria described above, a reasonably clean signal of D_s^\pm is observed (Fig. 3). The efficiency averaged over all momenta is $(40.5 \pm 1.0)\%$. It varies as a function of the D_s^\pm momentum and ranges from 30% when the D_s^\pm is at rest in the $\Upsilon(4S)$ rest frame to 55% for $p^* = 5 \text{ GeV}/c$. A clear signal of the Cabibbo-suppressed decay mode $D^\pm \rightarrow \phi\pi^\pm$ is also observed. A summary of the measured signal properties is given in the Table 1. The final production rates, however, are obtained from the invariant mass spectra fitted separately for different momentum intervals (Section 3.2). The measured mass difference $m_{D_s^\pm} - m_{D^\pm}$ agrees with the world average value of $99.2 \pm 0.5 \text{ MeV}/c^2$ [6].

Table 1: Fitted parameters for $D_s^\pm \rightarrow \phi\pi^\pm$ and $D_s^{*\pm} \rightarrow D_s^\pm\gamma$ decay modes.

	$D_s^\pm \rightarrow \phi\pi^\pm$	$D_s^{*\pm} \rightarrow D_s^\pm\gamma$
Fit	$N_{D_S} = 18269 \pm 202$ $M = 1968.5 \pm 0.1 \text{ MeV}/c^2$ $\sigma = 5.40 \pm 0.07 \text{ MeV}/c^2$ $M_{D_s^\pm} - M_{D^\pm} = 98.7 \pm 0.2 \text{ MeV}/c^2$	$N_{D_s^{*\pm}} = 3029 \pm 151$ $\Delta M = 143.4 \pm 0.3 \text{ MeV}/c^2$ $\sigma_{\Delta m} = 7.4 \pm 0.4 \text{ MeV}/c^2$

3.2 Inclusive D_s^\pm momentum spectra

The number of D_s^\pm mesons is extracted by fitting the $\phi\pi^\pm$ invariant mass distribution for different momentum ranges in the $\Upsilon(4S)$ rest frame. The momentum bin width is $200 \text{ MeV}/c$, which is much

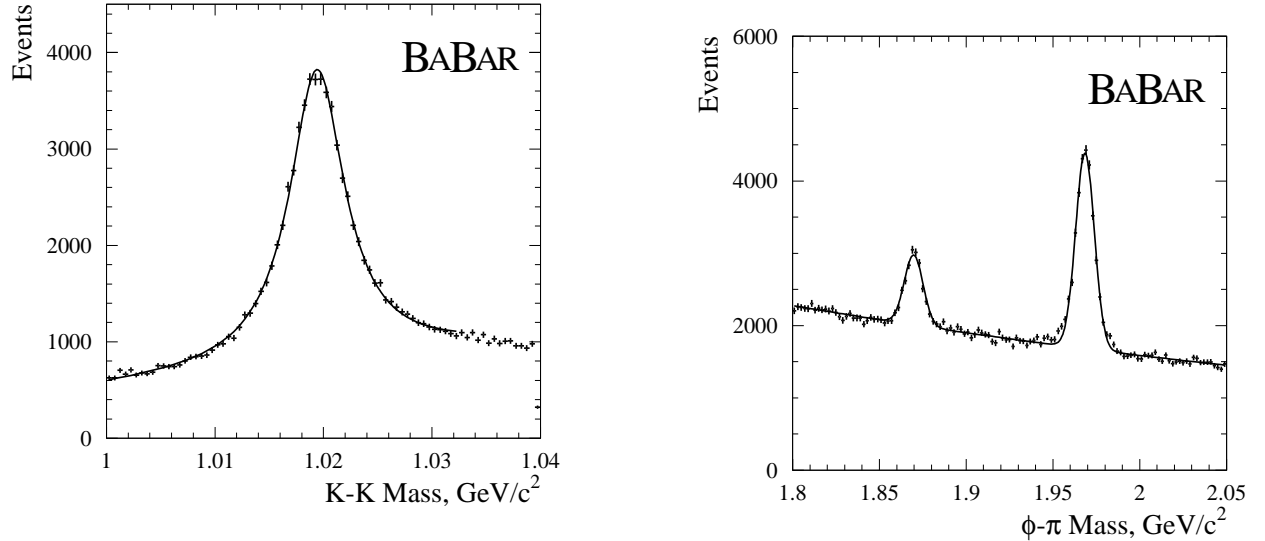


Figure 2: The K^+K^- invariant mass spectrum for an integrated luminosity of 1.53 fb^{-1} . The solid line represents a fit using a Breit-Wigner function and a 1st order polynomial.

Figure 3: The $\phi\pi$ invariant mass spectrum for an integrated luminosity of 7.73 fb^{-1} .

larger than the momentum resolution. The D_s^\pm momentum resolution averaged over all momenta obtained from the Monte Carlo is $5.6 \pm 0.3 \text{ MeV}/c$. The fit function is a single Gaussian distribution, both for the D_s^\pm and the D^\pm . The width of the Gaussians are constrained to be the same and the combinatorial background is accounted for by an exponential distribution. The number of D_s^\pm in the off-resonance data is extracted using the same fit function but with fixed values for M_{D^\pm} , $M_{D_s^\pm}$ and σ obtained from the fit to the on-resonance data.

The number of reconstructed D_s^\pm as a function of their momentum in the $\Upsilon(4S)$ rest frame is shown in Fig. 4 for on- and off-resonance data. The efficiency-corrected momentum spectrum is shown in Fig. 5.

Table 2: Analytical expressions for the fragmentation functions.

Name of function	Analytical expression
Peterson <i>et al.</i> :	$f(x_p) = \frac{N}{x_p} \left(1 - \frac{1}{x_p} - \frac{\epsilon}{1-x_p}\right)^{-2}$
Collins and Spiller:	$f(x_p) = N \left(\frac{1-x_p}{x_p} + \frac{2-x_p}{1-x_p}\epsilon\right) (1+x_p^2) \left(1 - \frac{1}{x_p} - \frac{\epsilon}{1-x_p}\right)^{-2}$
Kartvelishvili <i>et al.</i> :	$f(x_p) = Nx_p^\alpha(1-x_p)$

In order to determine the D_s^\pm momentum spectrum from the continuum, on-resonance data with momentum higher than $2.45 \text{ GeV}/c$ and off-resonance data scaled according to the luminosity ratio have been fitted after efficiency correction using 3 different fragmentation functions (see Table 2). The product of branching fraction, $\mathcal{B}(D_s^\pm \rightarrow \phi\pi^\pm)$, times cross-section for D_s^\pm production from continuum, $\sigma(e^+e^- \rightarrow D_s^\pm X)$, is obtained by integrating the function obtained from the fit (Fig. 5). The extracted values and χ^2/dof from the fits are shown in Table 3.

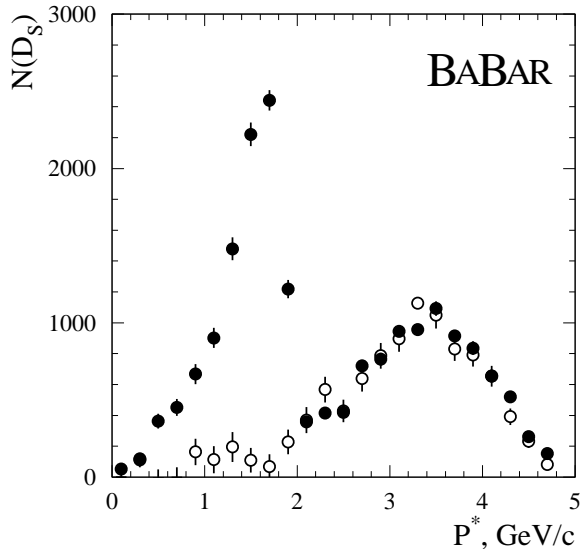


Figure 4: The D_s^\pm momentum spectrum for on-resonance data (solid circles) and for scaled off-resonance data (open circles) before efficiency correction.

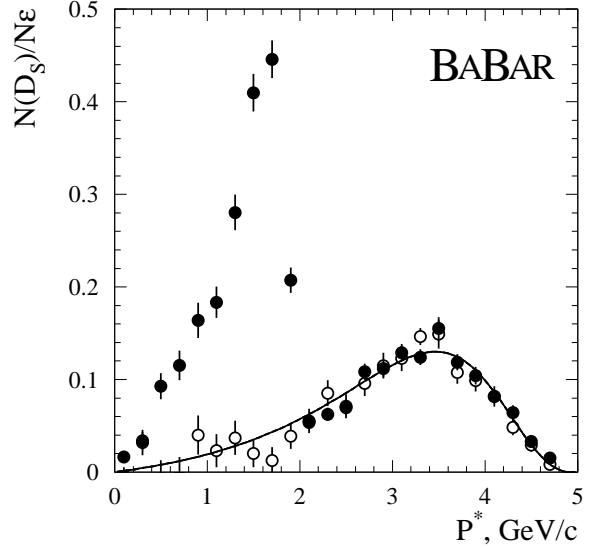


Figure 5: The on-resonance (solid circles) and scaled off-resonance (open circles) D_s momentum spectrum efficiency-corrected. The solid line is the result of the fit using Peterson fragmentation function described in text.

Table 4 shows the contribution of the different sources to the total systematic error for $\sigma(e^+e^- \rightarrow D_s^\pm X) \cdot \mathcal{B}(D_s^\pm \rightarrow \phi\pi^\pm)$. Using the best fit, which is obtained with the Peterson function, we find $\sigma(e^+e^- \rightarrow D_s^\pm X) \cdot \mathcal{B}(D_s^\pm \rightarrow \phi\pi^\pm) = 8.29 \pm 0.41 \pm 0.69$ pb. From a comparison of the results obtained using the other two parameterizations, we assign a conservative systematic error of 2% due to the assumed functional form.

The measured values are in good agreement with previously published results [7]. The momentum spectrum of the D_s produced in B decays is obtained by subtracting bin-by-bin the value of the fit function to the on-resonance data after efficiency correction (Fig. 6).

Table 3: The parameters for the different fragmentation functions obtained from the fit and the measured cross section $\sigma(e^+e^- \rightarrow D_s^\pm X) \cdot \mathcal{B}(D_s^\pm \rightarrow \phi\pi^\pm)$, and the χ^2/dof of the fit. Only the statistical errors are given.

Name of function	Shape parameter	$\sigma(e^+e^- \rightarrow D_s^\pm X) \cdot \mathcal{B}(D_s^\pm \rightarrow \phi\pi^\pm)$, pb	χ^2/dof
Peterson <i>et al.</i> :	$\epsilon = (12.5 \pm 0.6) \times 10^{-2}$	8.29 ± 0.41	1.286
Collins and Spiller:	$\epsilon = (37.6 \pm 2.8) \times 10^{-2}$	8.69 ± 0.46	3.559
Kartvelishvili <i>et al.</i> :	$\alpha = 1.91 \pm 0.07$	8.63 ± 0.33	5.338

Table 4: The systematic errors for $\sigma(e^+e^- \rightarrow D_s^\pm X) \cdot \mathcal{B}(D_s^\pm \rightarrow \phi\pi^\pm)$.

Source	Error (%)
$\mathcal{B}(\phi \rightarrow K^+K^-)$	1.6
Particle id efficiency	0.8
Tracking efficiency	7.5
Luminosity	3.0
Total systematic error	8.3

3.3 Inclusive D_s^\pm branching fraction in B decays

By integrating the efficiency corrected momentum distribution, a total D_s yield from B meson decays of 37050 ± 950 events is found. This corresponds to the inclusive branching fraction of

$$\mathcal{B}(B \rightarrow D_s^\pm X) = \left[(11.90 \pm 0.30 \pm 1.07) \times \frac{3.6 \pm 0.9\%}{\mathcal{B}(D_s^\pm \rightarrow \phi\pi^\pm)} \right] \%, \quad (1)$$

where the first error is statistical, the second is systematic and the third is the contribution of the $D_s^\pm \rightarrow \phi\pi^\pm$ branching fraction uncertainty [6]. Recognizing that this last uncertainty is common to all measurements, our result is slightly higher than the world average (10.0 ± 0.6 [6]) and in good agreement with the most precise measurement performed by CLEO [8]. The different sources of systematic errors are given in detail in Table 5. The dominant uncertainty comes from knowledge of the tracking efficiency, which is still the subject of detailed study [4].

As a cross check of the continuum subtraction procedure, we also subtracted directly the off-resonance data scaled by the luminosity ratio for on- and off-resonance. By this means, one obtains an inclusive branching fraction $\mathcal{B}(B \rightarrow D_s^\pm X) = 12.0 \pm 0.5 \pm 1.1\%$, in agreement with the value reported above.

4 Inclusive $D_s^{*\pm}$ production

4.1 $D_s^{*\pm}$ reconstruction

$D_s^{*\pm}$ mesons are reconstructed using the decay $D_s^{*\pm} \rightarrow D_s^\pm \gamma$ with the subsequent decay $D_s^\pm \rightarrow \phi\pi$. D_s^\pm candidates are selected by requiring the $\phi\pi$ invariant mass to be within 2.5 standard deviations (σ) of the peak value. These are then combined with “single photons” from the event. The latter are defined by the following criteria:

- $E_\gamma > 50$ MeV where E_γ is the photon energy in the laboratory frame
- $E_\gamma^* > 110$ MeV where E_γ^* is the photon energy in the $\Upsilon(4S)$ frame

Table 5: Systematic errors for $\mathcal{B}(B \rightarrow D_s^\pm X)$.

Source	Error (%)
Signal shape	0.9
Background shape	0.4
Continuum subtraction	1.8
Monte Carlo statistics	2.0
Bin width	0.7
Total for D_S yield	2.9
$N_{B\bar{B}}$	3.6
$\mathcal{B}(\phi \rightarrow K^+K^-)$	1.6
Particle id efficiency	0.8
Tracking efficiency	7.5
Total systematic error	9.0

Table 6: Systematic errors for $\mathcal{B}(B \rightarrow D_s^{*\pm} X)$.

Source	Error (%)
Signal shape	5.0
Continuum subtraction	1.2
Monte Carlo statistics	4.8
Bin width	3.0
Total for D_S yield	7.7
$N_{B\bar{B}}$	3.6
$\mathcal{B}(D_s^{*+} \rightarrow D_S \gamma)$	2.7
Photon efficiency	2.5
$\mathcal{B}(\phi \rightarrow K^+K^-)$	1.6
Particle id efficiency	0.8
Tracking efficiency	7.5
Total systematic error	12.0

- In order to reduce the combinatoric background, the candidate photon should not form a π^0 with $E_{\gamma\gamma}^* > 200$ MeV when combined with any other photon in the event. The π^0 mass window is $115 < M_{\gamma\gamma} < 155$ MeV/ c^2 .

The distribution of the mass difference $\Delta M = M_{D_s^\pm \gamma} - M_{D_s^\pm}$ is shown in the Fig. 7. A clear peak with 3030 ± 150 events is observed. The parameters obtained from the fit are summarized in Table 1.

4.2 Inclusive $D_s^{*\pm}$ momentum spectra

The decay $D_s^{*\pm} \rightarrow D_s^\pm \gamma$, $D_s^\pm \rightarrow \phi \pi^\pm$ is used for the measurement of the $D_s^{*\pm}$ inclusive branching fraction and the momentum spectrum. The number of $D_s^{*\pm}$ mesons is extracted by fitting the $\Delta M = M_{D_s \gamma} - M_{D_s}$ invariant mass distribution for the different momentum ranges in the $\Upsilon(4S)$ rest frame. A momentum bin width of 400 MeV/ c was chosen.

The efficiency corrected momentum spectrum is shown in Fig. 8. Both on- and off-resonance points corresponding to $D_s^{*\pm}$ mesons produced from the continuum have been fit using different fragmentation functions (Table 2). The cross section for $D_s^{*\pm}$ produced from continuum and the values of the fit parameters are shown in Table 7.

Fig. 9 shows the momentum spectrum of $D_s^{*\pm}$ produced in B decays where the Peterson fragmentation function is used for continuum extrapolation. Using this distribution, we find for the continuum cross section $\sigma(e^+e^- \rightarrow D_s^{*\pm} X) \cdot \mathcal{B}(D_s^\pm \rightarrow \phi \pi^\pm) = 3.48 \pm 0.39 \pm 0.38$ pb.

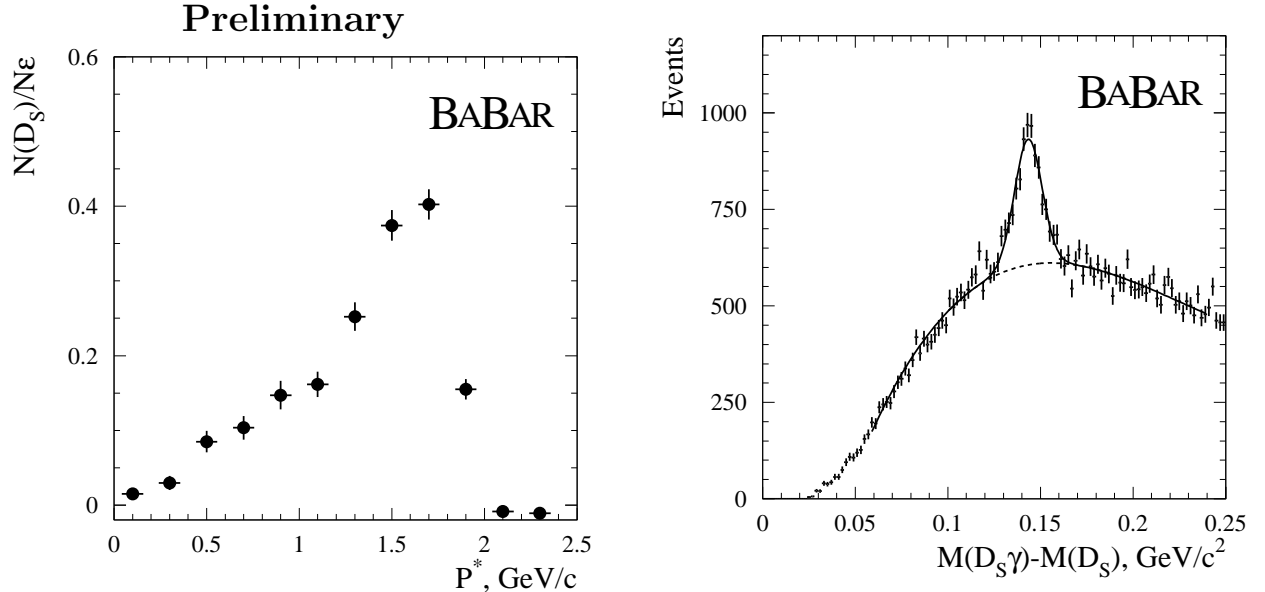


Figure 6: The D_s momentum spectrum efficiency-corrected after subtraction of the value of the fitted curve. The Peterson fragmentation function was used for the fit of the continuum.

Figure 7: $\Delta M = M_{D_s\gamma} - M_{D_s}$ mass spectrum for an integrated luminosity of 7.73 fb^{-1} . The fit function is a single Gaussian for the signal and a third-order polynomial for the background.

4.3 Inclusive $D_s^{*\pm}$ branching fraction in B decays

In the same way as for the D_s^\pm result, we integrate the efficiency corrected $D_s^{*\pm}$ distribution and obtain a total yield from B meson decays of 19300 ± 1900 events. From this we find the inclusive branching fraction to be

$$\mathcal{B}(B \rightarrow D_s^{*\pm} X) = \left[(6.8 \pm 0.7 \pm 0.8) \times \frac{3.6 \pm 0.9\%}{\mathcal{B}(D_s^\pm \rightarrow \phi\pi^\pm)} \right] \%, \quad (2)$$

where the systematic errors are given in detail in Table 6.

Table 7: The parameters for the different fragmentation functions, the measured cross section $\sigma(e^+e^- \rightarrow D_s^{*\pm} X) \cdot \mathcal{B}(D_s^\pm \rightarrow \phi\pi^\pm)$, and the χ^2/dof obtained from the fit. Only the statistical errors are given.

Name of function	Parameter	$\sigma(e^+e^- \rightarrow D_s^{*\pm} X) \cdot \mathcal{B}(D_s^\pm \rightarrow \phi\pi^\pm)$, pb	χ^2/dof
Peterson <i>et al.</i> :	$\epsilon = (7.9 \pm 0.8) \times 10^{-2}$	3.48 ± 0.39	1.260
Collins and Spiller:	$\epsilon = (19.3 \pm 2.3) \times 10^{-2}$	3.75 ± 0.42	1.288
Kartvelishvili <i>et al.</i> :	$\alpha = 2.6 \pm 0.2$	3.61 ± 0.29	1.725

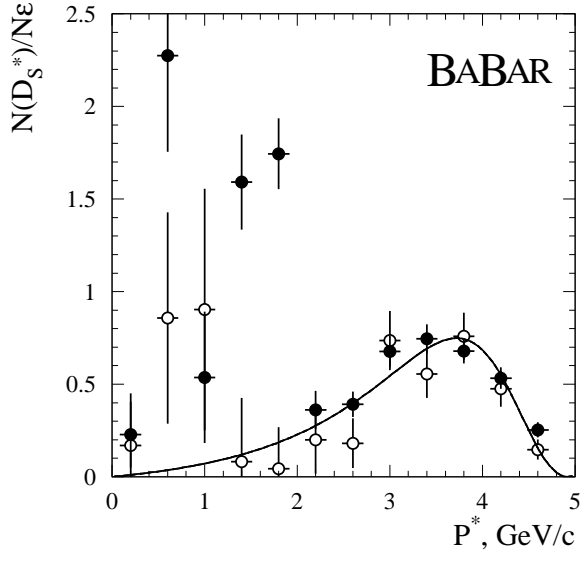


Figure 8: The on-resonance (solid circles) and scaled off-resonance (open circles) $D_s^{*\pm}$ momentum spectrum after efficiency correction. The solid line shows the fit using the Peterson fragmentation.

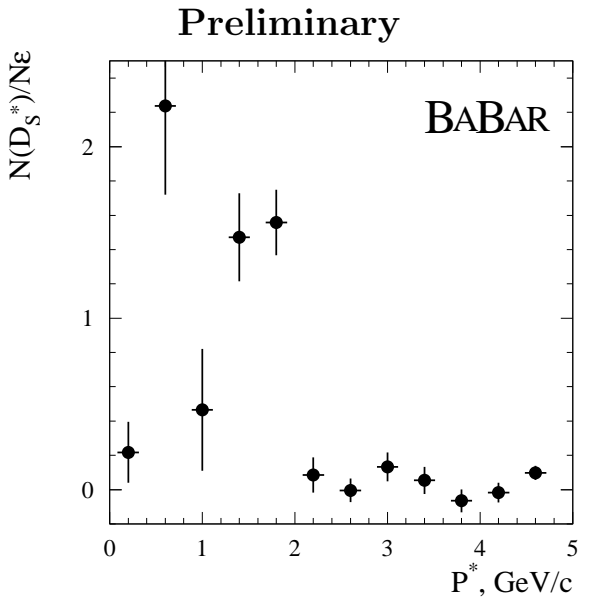


Figure 9: The $D_s^{*\pm}$ spectrum after efficiency correction and continuum subtraction using the result of the fit. The Peterson fragmentation function is used for the fit of the continuum.

5 Branching fraction for $B^0 \rightarrow D^{*-}D_s^{(*)+}$ decays

In addition to the measurements of inclusive production rates for D_s^\pm and $D_s^{*\pm}$, we have extracted the branching ratios for the decays $B^0 \rightarrow D^{*-}D_s^+$ and $B^0 \rightarrow D^{*-}D_s^{*+}$ based on a partial reconstruction method.

5.1 The partial reconstruction method

As discussed in the introduction, no attempt is made to reconstruct the D^0 decays. One combines a pion with the reconstructed $D_s^{(*)\pm}$ where the total $D_s^{(*)\pm} - \pi$ charge is zero and, assuming that their origin is a B^0 meson, we calculate the missing invariant mass. This should be the D^0 mass if the hypothesis is correct*. Without the constraint of the D^0 mass, the direction of the B meson is unknown. Although its angle with respect to D_s^\pm direction can be deduced, the angle ϕ around this direction is undetermined. Using the beam energy constraint, the missing mass, which still depending on the unknown angle ϕ of the B^0 momentum vector, is computed from:

$$m_{\text{miss}} = \sqrt{(E_{\text{beam}} - E_{D_s^\pm} - E_\pi)^2 - (\vec{p}_B - \vec{p}_{D_s^\pm} - \vec{p}_\pi)^2}. \quad (3)$$

In this analysis the missing mass is defined using an arbitrary choice for the angle ϕ . We use the convention that the direction of the B^0 meson lies in the plane $\{\vec{p}_\pi, \vec{p}_{D_s^{(*)\pm}}\}$.

* All calculations in this section are performed in the $\Upsilon(4S)$ rest frame.

5.2 Signal extraction

Fully reconstructed D_s^\pm and $D_s^{*\pm}$ are selected by requiring the measured $\phi\pi^\pm$ mass or $\Delta m = m_{\phi\pi^\pm\gamma} - m_{\phi\pi^\pm}$ to be within 2.5σ of the fitted mean value. Because of high combinatorial background in the mode with a $D_s^{*\pm}$, one may find several $D_s^{*\pm}$ candidates in an event. Therefore, we form a χ^2 for each candidate defined by:

$$\chi^2 = \left(\frac{M_\phi^{rec} - M_\phi^{mean}}{\sigma_\phi} \right)^2 + \left(\frac{M_{D_s}^{rec} - M_{D_s}^{mean}}{\sigma_{D_s}} \right)^2 + \left(\frac{M_{\Delta m}^{rec} - M_{\Delta m}^{mean}}{\sigma_{\Delta m}} \right)^2, \quad (4)$$

and take the candidate with the lowest value. The $D_s^{(*)\pm} - \pi$ pairs satisfying the kinematic constraints for the decay $B^0 \rightarrow D^* - D_s^{(*)+}$ are fitted to a common vertex. To reduce further the continuum background, we use the event shape variable R_2 , defined as the ratio of the second to zeroth order Fox-Wolfram moment, and require $R_2 < 0.35$.

The missing mass distributions for the $D_s^\pm - \pi$ and $D_s^{*\pm} - \pi$ are shown in Fig. 10 and 11 respectively. A clear signal is observed for both decays. The missing mass distribution is fitted with the sum of a Gaussian distribution for the signal and a background function given by

$$f_B(x) = \frac{C_1 (x_0 - x)^{C_2}}{C_3 + (x_0 - x)^{C_2}}, \quad (5)$$

where x is the calculated missing mass, C_i are the parameters of the fit and x_0 is the end point, $m_{D^*} - m_\pi = 1.871 \text{ GeV}/c^2$. The results of the fits for both decay modes are summarized in Table 8.

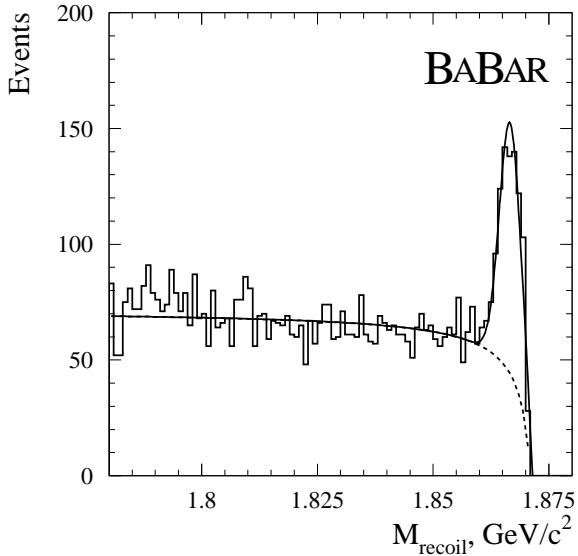


Figure 10: The missing mass distribution for the $D_s^\pm - \pi$ system. The solid line shows the result of the fit using the function described in the text.

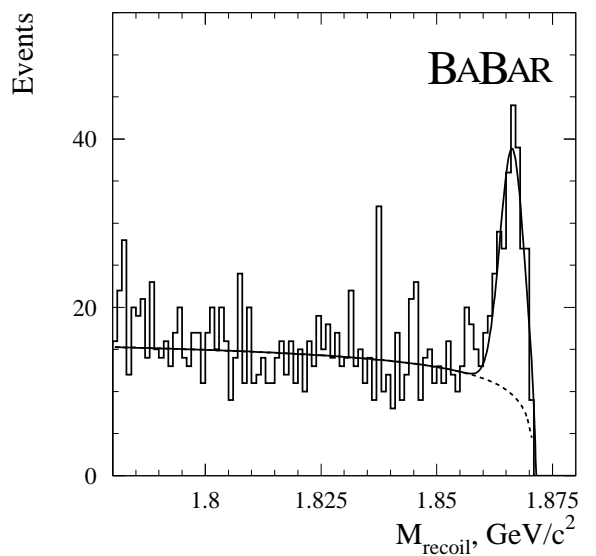


Figure 11: The missing mass distribution for the $D_s^{*\pm} - \pi$ system. The solid line shows the result of the fit using the function described in the text.

Table 8: Selection criteria and fit parameters for the missing mass distribution in partially reconstructed $B^0 \rightarrow D^{*-}D_s^{(*)+}$ decays.

$B \rightarrow D_s^+ D^{*-}$	$B \rightarrow D_s^{*+} D^{*-}$
$\chi^2/dof = 1.25$	$\chi^2/dof = 1.09$
$N_{\text{ev}} = 628 \pm 55$ events	$N_{\text{ev}} = 195 \pm 29$ events
$m_{\text{miss}} = 1866.7 \pm 0.2 \text{ MeV}/c^2$	$m_{\text{miss}} = 1866.3 \pm 0.2 \text{ MeV}/c^2$
$\sigma = 2.31 \pm 0.15 \text{ MeV}/c^2$	$\sigma = 2.66 \pm 0.36 \text{ MeV}/c^2$

5.3 Branching fractions for $B^0 \rightarrow D^{*-}D_s^+$ and $B^0 \rightarrow D^{*-}D_s^{*+}$

A Monte Carlo simulation of the $B^0 \rightarrow D^{*-}D_s^{(*)+}$ decay modes has been used to find the efficiencies. It is important to note that the $B^0 \rightarrow D^{*-}D_s^{*+}$ decay mode contributes to the missing mass distribution for the $D_s^\pm - \pi$ system, even though there is a missing photon from the $D_s^{*\pm}$. We show in Table 9 the reconstruction efficiencies for the different modes.

Table 9: The efficiencies for the partially reconstructed $B^0 \rightarrow D^{*-}D_s^{(*)+}$ decay modes. The columns show the contribution of the different generated modes to the $D_s^\pm - \pi$ and $D_s^{*\pm} - \pi$ missing mass distributions in the signal region.

True mode	Reconstructed mode	
	$D_s^\pm - \pi$	$D_s^{*\pm} - \pi$
$B^0 \rightarrow D^{*-}D_s^+$	$32.8 \pm 1.8\%$	
$B^0 \rightarrow D^{*-}D_s^{*+}$ long.pol.	$15.8 \pm 1.2\%$	$9.1 \pm 0.9\%$
$B^0 \rightarrow D^{*-}D_s^{*+}$ transv.pol.	$14.2 \pm 1.1\%$	$6.0 \pm 0.7\%$

Although the amount of feed through from $B^0 \rightarrow D^{*-}D_s^{*+}$ to $B^0 \rightarrow D^{*-}D_s^+$ depends on the $D_s^{*\pm}$ polarization, one sees from Table 9 that the variation is small. However the reconstruction efficiency for $B^0 \rightarrow D^{*-}D_s^{*+}$ has a much larger dependence on the polarization. Since this polarization is not known, we use the average efficiency of $(7.5 \pm 1.5)\%$, where the systematic error of 1.5% is derived by comparing the efficiencies from the two polarization states. This is combined with the other systematic errors which are in common with the inclusive branching fractions presented in the previous sections.

For the measurement of the $B^0 \rightarrow D^{*-}D_s^{*+}$ branching fraction, the contribution to the missing mass peak from $B^0 \rightarrow D^{*-}D_s^+$, where a random γ is associated to the D_s^\pm , is negligible. The contribution of $B^0 \rightarrow D^{*-}D_s^{*+}$ to the mode $B^0 \rightarrow D^{*-}D_s^+$ is then subtracted to determine the branching fraction for the latter. The results are given in Table 10. The first error is statistical, the third reflects the uncertainty due to the error in the branching ratio for $D_s^\pm \rightarrow \phi\pi^\pm$, and the second error represents all remaining systematics. This last is dominated by the uncertainty due

to the dependence of the efficiency on the polarization of the final state.

Table 10: The measured branching fraction for $B^0 \rightarrow D_s^{*-} D_s^+$ and $B^0 \rightarrow D_s^{*-} D_s^{*+}$.

Preliminary	
$B \rightarrow D_s^+ D_s^{*-}$	$B \rightarrow D_s^{*+} D_s^{*-}$
$\mathcal{B} = (7.1 \pm 2.4 \pm 2.5 \pm 1.8) \times 10^{-3}$	$\mathcal{B} = 2.54 \pm 0.38 \pm 0.53 \pm 0.64\%$
PDG: $\mathcal{B} = (9.6 \pm 3.4) \times 10^{-3}$	PDG: $\mathcal{B} = 2.0 \pm 0.7\%$

Finally, one should note that the reconstructed $B^0 \rightarrow D_s^{*-} D_s^{*+}$ events should allow us to measure the polarization of the $D_s^{*\pm}$ in these decays and therefore, in future analyses, it will be possible to reduce the systematic error from this source.

5.4 Background cross checks

In order to investigate further the shape of the background which is subtracted for estimating the signal, we have compared the Monte Carlo to the data. Several types of backgrounds contribute in the signal region:

1. Fake $D_s^{(*)\pm}$ and a random pion (for example coming from the other B).
2. Fake $D_s^{(*)\pm}$ and correlated pion (for example coming from the same B).
3. True $D_s^{(*)\pm}$ and a random pion.
4. True $D_s^{(*)\pm}$ and a correlated pion.

Table 11 shows the different types of backgrounds and the methods which are used to determine their level. Background types **1 + 3** are obtained by flipping the $D_s^{(*)\pm}$ direction. Background types **1 + 2** are extracted using the sidebands of the $D_s^{(*)\pm}$ mass distribution. For this purpose, we take $1.89 < M_{D_s^\pm} < 1.95$ and $1.985 < M_{D_s^\pm} < 2.05$ GeV/ c^2 for the $D_s^\pm - \pi$ system, and $\Delta M_{D_s^{*\pm}} < 170 < \Delta M_{D_s^{*\pm}} < 300$ MeV/ c^2 for $D_s^{*\pm} - \pi$. By flipping the $D_s^{(*)\pm}$ direction for the sidebands we find the contribution of background type **1**. Therefore the difference between the distributions for flipped and non-flipped $D_s^{(*)\pm}$ direction for the sidebands gives the type **2** background contribution and thus it is possible to find the contribution of background types **1 + 2 + 3** from data alone. Fig. 12 and 13 show the resulting signal after their subtraction. The remaining background component is quite small and is estimated from the Monte Carlo. To ensure that the simulation reproduce the data well, a systematic comparison is made for the missing mass distribution obtained from the D_s^\pm signal region, the D_s^\pm sideband region, and the wrong-sign $D_s^\pm - \pi$ combinations both in the D_s^\pm signal and the D_s^\pm sideband regions. The ratio (Data-Monte Carlo)/Monte Carlo for all these cases are determined as a function of the missing mass. We find good agreement within the errors in all cases. Table 12 summarizes this result by showing the ratio integrated over the missing mass region 1.78 to 1.87 GeV/ c^2 for all distributions except that with the signal, for which the range 1.78 to 1.85 GeV/ c^2 is used.

Table 11: The different data samples which can be used to determine the background in the D^0 signal region.

Background	Flip $D_s^{(*)\pm}$	$D_s^{(*)\pm}$	Side-bands	Side-bands flip $D_s^{(*)\pm}$
1. Fake $D_s^{(*)\pm}$ + random π	x		x	x
2. Fake $D_s^{(*)\pm}$ + correlated π			x	
3. True $D_s^{(*)\pm}$ + random π		x		
4. True $D_s^{(*)\pm}$ + correlated π				

Table 12: The comparison of the different data samples with Monte Carlo.

Sample type	$B^0 \rightarrow D^{*-} D_s^+$		$B^0 \rightarrow D^{*-} D_s^{*+}$	
	$(N_{\text{data}} - N_{\text{MC}})/N_{\text{MC}}$	χ^2/dof	$(N_{\text{data}} - N_{\text{MC}})/N_{\text{MC}}$	χ^2/dof
D_s^\pm Signal	0.051 ± 0.025	1.008	0.103 ± 0.057	1.058
Flip D_s^\pm	-0.043 ± 0.031	0.841	-0.041 ± 0.064	0.832
D_s^\pm Sideband	0.006 ± 0.018	1.391	-0.031 ± 0.053	1.194
Flip D_s^\pm Sideband	0.015 ± 0.021	1.627	0.084 ± 0.069	1.690
Wrong Sign	-0.031 ± 0.029	0.987	0.010 ± 0.063	1.088
WS, D_s^\pm Sideband	0.030 ± 0.020	1.311	0.034 ± 0.065	1.487

6 Conclusion

The production of $D_s^{(*)\pm}$ at the $\Upsilon(4S)$ energy (and 40 MeV below) has been studied with the *BABAR* detector. Preliminary measurements of branching fractions for the inclusive production and for the exclusive decays $B^0 \rightarrow D^{*-} D_s^{*+}$ have been performed. The following cross sections have been found for production in the continuum:

$$\sigma(e^+e^- \rightarrow D_s^\pm X) \cdot \mathcal{B}(D_s^\pm \rightarrow \phi\pi^\pm) = 8.29 \pm 0.41 \pm 0.69 \text{ pb ,}$$

$$\sigma(e^+e^- \rightarrow D_s^{*\pm} X) \cdot \mathcal{B}(D_s^{*\pm} \rightarrow \phi\pi^\pm) = 3.48 \pm 0.39 \pm 0.38 \text{ pb .}$$

Using the on-resonance data, the inclusive branching fraction for the B meson decays

$$\begin{aligned} \mathcal{B}(B \rightarrow D_s^\pm X) &= \left[(11.90 \pm 0.30 \pm 1.07) \times \frac{3.6 \pm 0.9\%}{\mathcal{B}(D_s^\pm \rightarrow \phi\pi^\pm)} \right] \% \\ \mathcal{B}(B \rightarrow D_s^{*\pm} X) &= \left[(6.8 \pm 0.7 \pm 0.8) \times \frac{3.6 \pm 0.9\%}{\mathcal{B}(D_s^{*\pm} \rightarrow \phi\pi^\pm)} \right] \% \end{aligned}$$

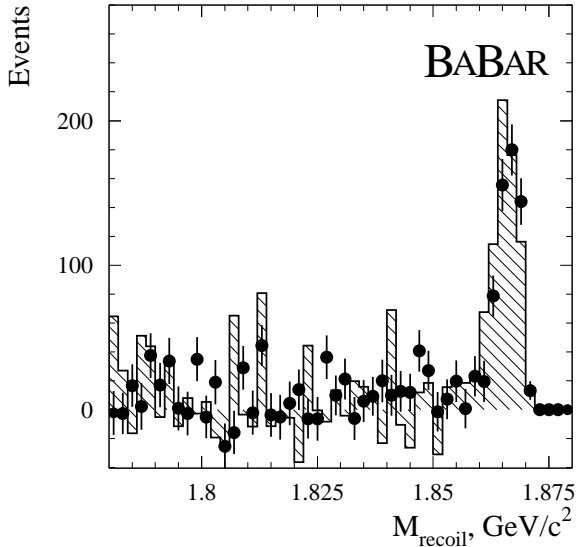


Figure 12: The missing mass distribution for the $D_s^{\pm}-\pi$ system from data (points) and Monte Carlo (histogram) after background subtraction (see text).

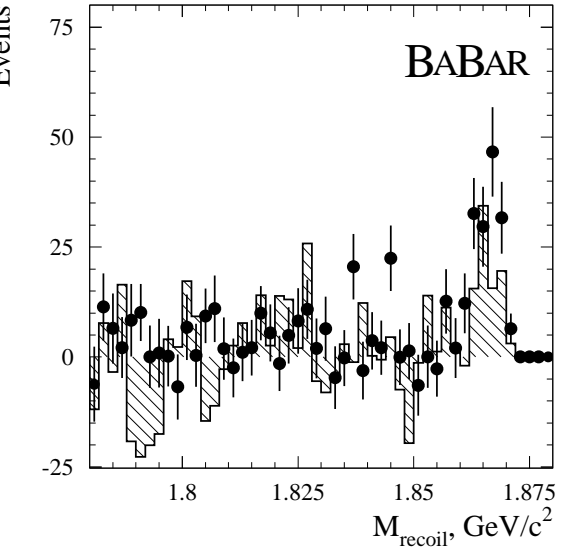


Figure 13: The missing mass distribution for $D_s^{*\pm}-\pi$ system from data (points) and Monte Carlo (histogram) after background subtraction (see text).

have been measured. Finally the decays $B^0 \rightarrow D^{*-}D_s^+$ and $B^0 \rightarrow D^{*-}D_s^{(*)+}$ have been observed using a partial reconstruction technique and the following branching fractions have been determined:

$$\begin{aligned}\mathcal{B}(B \rightarrow D_s^+ D^{*-}) &= (7.1 \pm 2.4 \pm 2.5 \pm 1.8) \times 10^{-3}, \\ \mathcal{B}(B \rightarrow D_s^{*+} D^{*-}) &= (2.54 \pm 0.38 \pm 0.53 \pm 0.64)\%.\end{aligned}$$

The results obtained are in a good agreement with previous measurements by other experiments. The measurement of inclusive branching fraction of $D_s^{*\pm}$ from B decay has been obtained for the first time.

7 Acknowledgements

We are grateful for the contributions of our PEP-II colleagues in achieving the excellent luminosity and machine conditions that have made this work possible. We acknowledge support from the Natural Sciences and Engineering Research Council (Canada), Institute of High Energy Physics (China), Commissariat à l’Energie Atomique and Institut National de Physique Nucléaire et de Physique des Particules (France), Bundesministerium für Bildung und Forschung (Germany), Istituto Nazionale di Fisica Nucleare (Italy), The Research Council of Norway, Ministry of Science and Technology of the Russian Federation, Particle Physics and Astronomy Research Council (United Kingdom), the Department of Energy (US), and the National Science Foundation (US). In addition, individual support has been received from the Swiss National Foundation, the A. P. Sloan Foundation, the Research Corporation, and the Alexander von Humboldt Foundation. The visiting groups wish to thank SLAC for the support and kind hospitality extended to them.

References

- [1] A. F. Falk, M. B. Wise and I. Dunietz, Phys. Rev. **D 51** (1995) 1183.
- [2] I. Bigi *et al.*, Phys. Lett. **B 323** (1994) 408.
- [3] R. Aleksan, M. Zito, A. Le Yaouanc, L. Oliver, O. Péne and J.-C. Raynal, Preprint hep-ph/9906504; also LPT-ORSAY-99-35 and DAPNIA-SPP-99-18, May 1999.
- [4] BABAR Collaboration, B. Aubert *et al.*, “The first year of the *BABAR* experiment at PEP-II”, BABAR-CONF-00/17, submitted to the XXXth International Conference on High Energy Physics, Osaka, Japan.
- [5] P. F. Harrison and H. R. Quinn, eds., “The *BABAR* physics book”, SLAC-R-405 (1998).
- [6] Particle Data Group, *Review of Particle Properties*, Phys. Rev. **D 54** (1996) 1.
- [7] ARGUS Collaboration, H. Albrecht *et al.*, Z. Phys. **C 54** (1992) 1.
- [8] CLEO Collaboration, D. Gibaut *et al.*, Phys. Rev. **D 53** (1996) 4734.